Local density of optical states calculated by the mode spectrum in stratified media

Ting Fu(傅廷)[1,3], Jingxuan Chen(陈静瑄)[1,3], Xueyou Wang(王学友)[1], Yingqiu Dai(戴迎秋)[1,2], Xuyan Zhou(周旭彦)[1,5,†], Yufei Wang(王宇飞)[1,2,‡], Mingjin Wang(王明金)[1], and Wanhua Zheng(郑婉华)[1,2,3,4,§]

[1] *Laboratory of Solid State Optoelectronics Information Technology, Institute of Semiconductors, Chinese Academy of Sciences, Beijing* 100083, *China*
[2] *College of Future Technology, University of Chinese Academy of Sciences, Beijing* 101408, *China*
[3] *Center of Materials Science and Optoelectronics Engineering, University of Chinese Academy of Sciences, Beijing* 100049, *China*
[4] *State Key Laboratory on Integrated Optoelectronics, Institute of Semiconductors, Chinese Academy of Sciences, Beijing* 100083, *China*
[5] *Weifang Academy of Advanced Opto-electronic Circuits, Weifang* 261021, *China*

(Received 22 September 2022; revised manuscript received 16 December 2022; accepted manuscript online 30 December 2022)

The local density of optical states (LDOS) is an important physical concept, which can characterize the spontaneous emission of microcavities. In order to calculate the LDOS, the relationship between the mode spectrum and the LDOS is established. Then, based on the transfer matrix method and the effective resonator model, the leaky loss of the leaky mode and the mode spectrum in the one-dimensional photonic bandgap crystal waveguide are calculated, results of which indicate that the mode spectrum can characterize the leaky loss of the leaky mode. At last, the density of optical states (DOS), and the LDOS in each layer are calculated. The partial DOS and the partial LDOS in the quantum well, related to the fundamental leaky mode, can be used to find out the optimal location of the quantum well in the defect layer to couple more useful photons into the lasing mode for lasers.

Keywords: local density of optical states, mode spectrum, transfer matrix method

PACS: 02.60.Cb, 42.25.Bs, 42.60.Da **DOI:** 10.1088/1674-1056/acaf2c

1. Introduction

The spontaneous emission is an important radiative recombination process in semiconductor devices, ranging from laser diodes to light emitting diodes,[1,2] which can be controlled by the environment surrounding the active emitter.[3] According to the Fermi's golden rule, the spontaneous emission rate is proportional to the local density of optical states (LDOS),[4–6] which contains the influences of the density of optical states (DOS) and the electric field on the active emitter simultaneously.[7] Therefore, compared with the DOS, the LDOS can characterize the spontaneous radiative emission rate at every position of microcavities while the DOS, which is the integral of the LDOS over space, loses the information of positions in the microcavities.[8] The LDOS has been widely used to investigate the spontaneous radiative characteristics in optical devices such as lasers,[7,9] nanocavities,[10–12] photonic crystals,[13–16] and so on. There are also many ways to measure the LDOS, such as cathodoluminescence microscopy,[17–19] time-resolved measurements,[6] *etc.* Besides, many methods have been adopted to calculate the LDOS. For example, the Green's function is a common way to calculate the LDOS of photonic crystals.[8,14,20] The plane-wave expansion is also explored to calculate the LDOS of two-dimensional (2D) photonic crystals.[7,21] However, little research has been conducted to calculate the LDOS of one-dimensional (1D) arbitrary stratified media.[13–15,22] Therefore, a method based on the effective resonator model (ERM) is proposed to calculate the LDOS in 1D multi-layer waveguides in this work.

In this paper, recent progresses in the LDOS are reviewed at the beginning. In Section 2, the relationship between mode spectrum and LDOS is established mathematically. In Section 3, the numerically calculated results are discussed. In Section 4, a conclusion is offered.

2. Theory and design

The ERM can convert the 1D multi-layer waveguide to an effective Fabry–Pérot (FP) resonator,[23–26] as shown in Fig. 1(a). For the layer i in the waveguide, a plane wave $E_0 = C_0 \exp[-\mathrm{i}k_{i,x}(x - x_i)]$ is incident on this layer to stimulate the effective plane wave E_R in the effective FP resonator, where C_0 is the amplitude coefficient of the electric field, $k_{i,x}$ is the x component of the wave vector in the layer i, and x_i is the boundary between the layer i and layer $i+1$. The effective FP resonator has two mirrors with the reflection coefficients of r_L and r_R respectively, which can reflect the incident wave back and forth, as shown in Fig. 1(b). When the incident light is firstly reflected by the right mirror, the reflected wave arriving

†Corresponding author. E-mail: zhouxuyan@semi.ac.cn
‡Corresponding author. E-mail: yufeiwang@semi.ac.cn
§Corresponding author. E-mail: whzheng@semi.ac.cn

© 2023 Chinese Physical Society and IOP Publishing Ltd

at the left mirror can be expressed as

$$E_0' = r_{\mathrm{R}} C_0 \exp\left(-\mathrm{i}2k_{i,x}d_i\right)\exp\left[\mathrm{i}k_{i,x}\left(x-x_i\right)\right], \tag{1}$$

where d_i is the thickness of the layer i. After E_0' is reflected by the left mirror, the reflected wave can be expressed as

$$E_1 = r_{\mathrm{L}} r_{\mathrm{R}} C_0 \exp\left(-\mathrm{i}2k_{i,x}d_i\right)\exp\left[-\mathrm{i}k_{i,x}\left(x-x_i\right)\right]. \tag{2}$$

Besides, the incident wave satisfies the continuity condition on the left mirror,[24,25] so two similar plane waves would be stimulated in the cavity and can be described as

$$E_{-1}' = r_{\mathrm{L}}^* C_0 \exp\left[\mathrm{i}k_{i,x}\left(x-x_i\right)\right], \tag{3}$$

$$E_{-1} = r_{\mathrm{L}}^* r_{\mathrm{R}}^* C_0 \exp\left(\mathrm{i}2k_{i,x}d_i\right)\exp\left[-\mathrm{i}k_{i,x}\left(x-x_i\right)\right], \tag{4}$$

where the asterisk stands for the conjugation. Then, the right-traveling wave in the cavity can be summed and expressed as

$$\begin{aligned} E_{\mathrm{R}} &= E_0 + E_1 \sum_{j=0}^{\infty}\left[r_{\mathrm{L}} r_{\mathrm{R}} \exp\left(-\mathrm{i}2k_{i,x}d_i\right)\right]^j \\ &\quad + E_{-1} \sum_{j=0}^{\infty}\left[r_{\mathrm{L}}^* r_{\mathrm{R}}^* \exp\left(\mathrm{i}2k_{i,x}d_i\right)\right]^j. \end{aligned} \tag{5}$$

Likewise, the left-traveling wave can be expressed as

$$\begin{aligned} E_{\mathrm{L}} &= E_0' \sum_{j=0}^{\infty}\left[r_{\mathrm{L}} r_{\mathrm{R}} \exp\left(-\mathrm{i}2k_{i,x}d_i\right)\right]^j \\ &\quad + E_{-1}' \sum_{j=0}^{\infty}\left[r_{\mathrm{L}}^* r_{\mathrm{R}}^* \exp\left(\mathrm{i}2k_{i,x}d_i\right)\right]^j. \end{aligned} \tag{6}$$

If the operator $\boldsymbol{Q}$ stands for the operation of the effective resonator on the incident wave E_0, then, the eigen-equation of the resonator can be established as

$$\boldsymbol{Q}E_0 = \Lambda E_0, \tag{7}$$

where the incident wave E_0 is called a mode of the resonator and Λ is the corresponding eigenvalue. The operator $\boldsymbol{Q}$ would relate incident plane wave E_0 with the effective plane wave E_{R}, which means that $E_{\mathrm{R}} = \boldsymbol{Q}E_0$. Therefore, the eigenvalue Λ shows the probability of the existence of specific modes in the resonator and is related to the mode spectrum, which is the angular distribution of modes in the wave vector space.[23,27] According to Eqs. (5) and (7) and the mode spectrum in vacuum,[23,25] the mode spectrum in the effective cavity can be expressed as

$$\rho_{\mathrm{ms}} = \frac{1}{8\pi^3}\frac{1-\left|r_{\mathrm{L}} r_{\mathrm{R}}\right|^2}{1+\left|r_{\mathrm{L}} r_{\mathrm{R}}\right|^2 - 2\mathrm{Re}\left[r_{\mathrm{L}} r_{\mathrm{R}} \exp\left(-\mathrm{i}2k_{i,x}d_i\right)\right]}, \tag{8}$$

where Re represents the real part of a complex number. Here, the reflection coefficients r_{L} and r_{R} can be calculated by the transfer matrix method (TMM) and expressed as[28]

$$r_{\mathrm{L,R}} = \left(\frac{M_{21}}{M_{11}}\right)_{\mathrm{L,R}}, \tag{9}$$

where M_{21} and M_{11} are the elements of the translation matrix of the multi-layer waveguides on each side of the effective resonator.[28] Then, the number of modes in wave vector space of $\mathrm{d}k_i$ can be described as

$$\mathrm{d}N\left(k_i\right) = k_i^2\,\mathrm{d}k_i \int_{4\pi} \rho_{\mathrm{ms}}\left(\boldsymbol{k}_i\right)\mathrm{d}\Omega, \tag{10}$$

where k_i is the absolute value of the wave vector $\boldsymbol{k}_i$ of layer i, and the integral covers all solid angles.[23] Here, only the transverse electric (TE) wave is considered, so equation (10) does not incorporate the contribution of polarizations. The DOS ρ_{p} in the angular frequency domain is related to the mode spectrum by $\mathrm{d}N/\mathrm{d}\omega$ and can be expressed as

$$\rho_{\mathrm{p}}\left(\omega\right) = \frac{k_0^2 n_i^3}{c}\int_{4\pi} \rho_{\mathrm{ms}}\left(\boldsymbol{k}_i\right)\mathrm{d}\Omega, \tag{11}$$

where ω is the angular frequency, k_0 is the wave vector in vacuum, n_i is the refractive index of the layer i, and c is the speed of the light in vacuum.

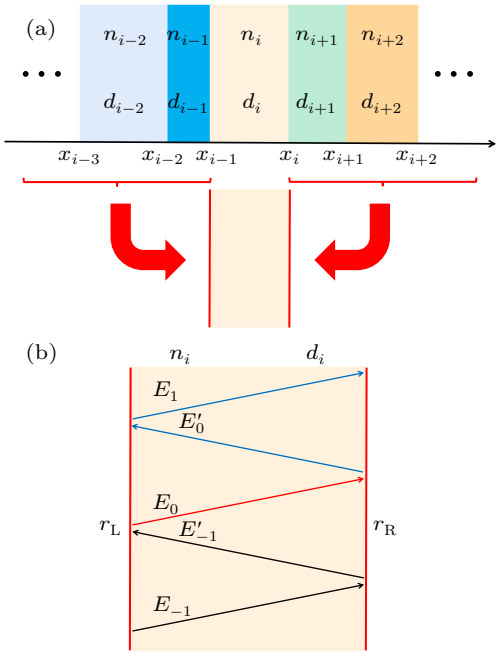


Fig. 1. (a) The schematic diagram of the conversion of the stratified medium to an effective FP resonator. (b) The process of the light propagation in the effective FP cavity stimulated by the plane wave E_0.

Although the DOS defined by Eq. (11) can reveal the average number of available modes in the effective resonator, it does not contain the spatial dependence of the number of modes inside the resonator. According to weighting the mode spectrum by the intensity of the eigenmodes in the process of the DOS calculation, the LDOS in the resonator can be obtained, which is able to describe the local availability of modes coupled to active emitters.[27,29] Therefore, the electric field in the resonator has to be determined and can be calculated by $E_i = E_{\mathrm{L}} + E_{\mathrm{R}}$ based on Eqs. (5) and (6). After some simplifications, the effective distribution of the electric field can be expressed as

$$E_i\left(\boldsymbol{k}_i, x\right) = C_0 \rho_{\mathrm{ms}}\left(\boldsymbol{k}_i\right)\left[\exp\left(-\mathrm{i}k_{ix}\left(x-x_i\right)\right)\right.$$

$$+\exp\left(\mathrm{i}k_{ix}\left(x-x_i\right)\right)\xi^*\left(\boldsymbol{k}_i\right)\Big], \tag{12}$$

where the influence of $1/(8\pi^3)$ is ignored, because it can be incorporated into the constant C_0, and $\xi(\boldsymbol{k}_i)$ is the coupling function defined as[24]

$$\xi\left(\boldsymbol{k}_i\right)=\frac{r_{\mathrm{R}}^*\left(1-\left|r_{\mathrm{L}}\right|^2\right)\exp\left(\mathrm{i}2k_{ix}d_i\right)+r_{\mathrm{L}}\left(1-\left|r_{\mathrm{R}}\right|^2\right)}{1-\left|r_{\mathrm{L}}r_{\mathrm{R}}\right|^2}. \tag{13}$$

Then, the electric field in the whole multi-layer waveguide can be obtained by applying the continuity conditions of the tangential components of the electromagnetic fields at the interfaces between adjacent layers.[24] Equations (11) and (12) indicate that the DOS defined by Eq. (11) already includes the difference among different layers according to the mode spectrum, which contains the partial information of the electric field, as shown by Eq. (12). Therefore, the electric fields of optical modes can be normalized separately in each layer.[8,30] Here, for the layers with a finite thickness in the 1D waveguide, the electric field in the effective resonator is normalized according to[30]

$$\int_{x_{i-1}}^{x_i}\left|E\left(\boldsymbol{k}_i,x\right)\right|^2\mathrm{d}x=1. \tag{14}$$

If the electric field is not normalized, the electric field must be divided by a normalization constant, which can be written as

$$C_1=\sqrt{\int_{x_{i-1}}^{x_i}\left|E\left(\boldsymbol{k}_i,x\right)\right|^2\mathrm{d}x}. \tag{15}$$

By incorporating Eq. (14) into Eq. (11), the DOS can be further expressed as

$$\rho_{\mathrm{p}}\left(\omega\right)=\frac{1}{u_i}\int_{x_{i-1}}^{x_i}\left[\frac{u_ik_0^2n_i^3}{c}\int_{4\pi}\rho_{\mathrm{ms}}\left(\boldsymbol{k}_i\right)\left|E_i\left(\boldsymbol{k}_i,x\right)\right|^2\mathrm{d}\Omega\right]\mathrm{d}x, \tag{16}$$

where u_i is a normalization factor. The relationship between the DOS and the LDOS can be expressed as[8]

$$\rho_{\mathrm{p}}\left(\omega\right)=\frac{1}{u_i}\int_{x_{i-1}}^{x_i}\rho_{\mathrm{l}}\left(\omega,x\right)\mathrm{d}x. \tag{17}$$

By comparing Eq. (16) with Eq. (17), the LDOS in the layer i of the 1D multi-layer waveguide can be defined as

$$\rho_{\mathrm{l}}\left(\omega,x\right)=\frac{u_ik_0^2n_i^3}{c}\int_{4\pi}\rho_{\mathrm{ms}}\left(k_i\right)\left|E_i\left(k_i,x\right)\right|^2\mathrm{d}\Omega, \tag{18}$$

where the normalization factor u_i in the 1D resonator is defined as

$$u_i=d_i, \tag{19}$$

so that the right side of Eq. (18) can be reduced to $\omega^2n_i^3/(2\pi^2c^3)$ in the case of uniform media. Considering that $k_{i,x}=k_0n_i\cos\theta$, where θ is the angle between the incident wave and the positive x axis, and the 1D multi-layer waveguide exhibits the rotational symmetry in the plane perpendicular to the x axis, equation (18) can be simplified to

$$\rho_{\mathrm{l}}\left(\omega,x\right)=\frac{u_ik_0^2n_i^3}{4\pi^2c}\int_0^{\pi}\frac{\sin\theta\left(1-\left|r_{\mathrm{L}}r_{\mathrm{R}}\right|^2\right)}{1+\left|r_{\mathrm{L}}r_{\mathrm{R}}\right|^2-2\mathrm{Re}\left[r_{\mathrm{L}}r_{\mathrm{R}}\exp\left(-\mathrm{i}2k_0n_id_i\cos\theta\right)\right]}\left|E_i\left(\omega,\theta,x\right)\right|^2\mathrm{d}\theta. \tag{20}$$

For the outmost layers of the 1D multi-layer waveguide, equation (20) is still valid for radiation modes if the normalization of the electric field and the normalization factor are corrected properly. Take the first layer in the waveguide as an example. Because of the semi-infinite distribution of the electric field in this layer, the electric field can be normalized by the Dirac function,[31] and expressed as

$$\int_{-\infty}^{x_1}E\left(\boldsymbol{k}_1,x\right)E^*\left(\boldsymbol{k}_1',x\right)\mathrm{d}x=\delta\left(k_{1,x}-k_{1,x}'\right), \tag{21}$$

where $\delta(k_{1,x}-k_{1,x}')=0$, when $k_{1,x}\neq k_{1,x}'$; $\delta(k_{1,x}-k_{1,x}')=\infty$, when $k_{1,x}=k_{1,x}'$. If the electric field is not normalized, the electric field must be divided by a corrected normalization constant. The normalization constant of the first layer can be expressed as[31,32]

$$C_1=\sqrt{\pi\left(\left|a_1\right|^2+\left|b_1\right|^2\right)}, \tag{22}$$

where a_1 and b_1 are the amplitude coefficients of electric fields of the right-travelling wave and the left-travelling wave at the boundary of x_1, respectively. In the case of uniform media, the optical mode is simply a plane wave in the first layer, which is in the form of $\exp[-\mathrm{i}k_{1,x}(x-x_1)]/\pi^{0.5}$. The LDOS in the first layer must be also reduced to $\omega^2n_1^3/(2\pi^2c^3)$ in the case of uniform media, so the normalization factor u_i in Eq. (18) should be corrected as π for the outmost layers. For the last layer, similar results can be obtained. Then, based on Eqs. (12) and (20) with u_i defined in each layer, the LDOS in each layer of the stratified waveguide can be calculated.

Here, the DOS and the LDOS in the epitaxy of the longitudinal photonic bandgap crystal (PBC) laser[33–35] with center wavelength of 980 nm are calculated. The epitaxial structure of the PBC waveguide is shown in Fig. 2(a), including air, contact layer, P-cladding layer, defect layer, active layer inserted in the defect layer, finite PBC, N-cladding layer, and substrate.[36] For the PBC waveguide, the fundamental mode of the defect layer is located at the allowed band edge of the PBC, which is good for larger mode volumes and enhanced mode discrimination. Figure 2(b) is the corresponding distribution of the refractive index of the PBC waveguide. The inset

in Fig. 2(b) shows that the active layer, inserted in the defect layer, is composed of two quantum barriers and one quantum well (QW).

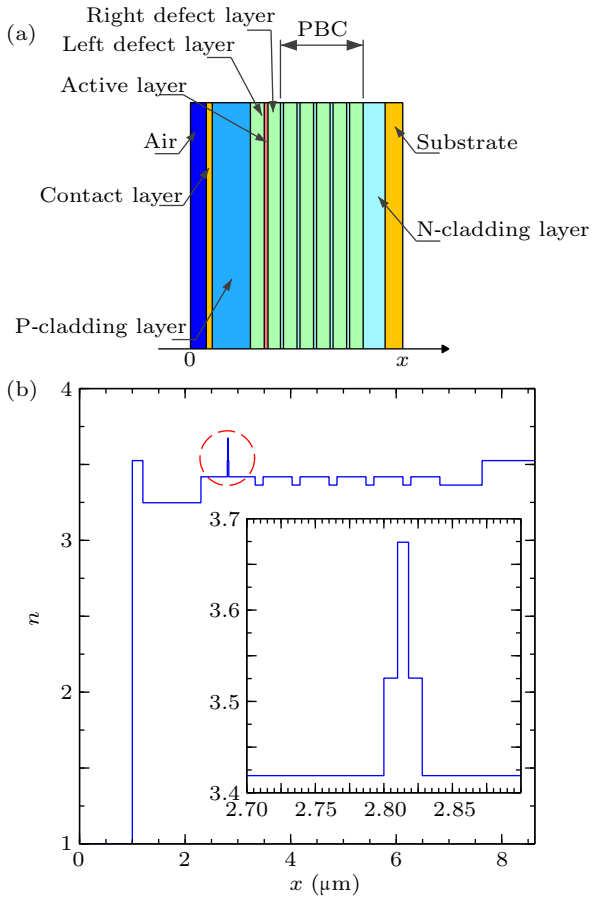


Fig. 2. (a) The schematic diagram of the 1D PBC waveguide to be studied. (b) The distribution of the refractive index of the waveguide. The inset is the enlarged image of the region indicated by the red dashed circle, which shows that the active layer inserted in the defect layer is composed of two quantum barriers and one quantum well.

3. Results and discussion

3.1. Leaky modes and mode spectra

For the PBC waveguide shown in Fig. 2, the electric field and the mode spectrum in each layer must be determined in order to calculate the DOS and the LDOS. At first, the leaky modes in the PBC waveguide are calculated by the TMM to be compared with the results of the ERM. Because there is a substrate layer in the PBC waveguide, the refractive index of which is higher than the effective refractive index of any guided modes for the same PBC waveguide without the substrate layer, only the radiation modes exist in the PBC waveguide with the substrate layer. Mathematically, there are also leaky modes in the PBC waveguide, which can characterize the quality factors of the resonances in the waveguide, even though the leaky modes are not the eigenmodes of the waveguide.[37,38] By imposing the outgoing-wave boundary conditions on the outmost layers,[39] the distributions of the electric fields and the complex propagation constants of the leaky modes are calculated by the TMM. The wavelength is fixed at 980 nm. The red solid line in Fig. 3(a) is the distribution of the normalized electric field of fundamental leaky mode, which is mainly confined in the defect layer. Therefore, the fundamental leaky mode possesses the smallest leaky loss, as indicated by the blue square point in Fig. 3(b). Figure 3(b) depicts the distributions of the complex propagation constants of the first six leaky modes. The real part of the complex propagation constant stands for the propagation constant β_r, which is related to the propagation direction of the leaky mode. The imaginary part of the complex propagation constant stands for the leaky loss. From Fig. 3(b), it can be known that the higher the order of the leaky mode is, the larger the leaky loss is, also suggested by the second column of Table 1.

Table 1. Calculated results around the mode angles of the leaky modes in the QW.

θ_{leaky} (°)	Im(β) (cm^{-1})	FWHM (°)	$\rho_{\text{ms,max}}$	$\rho_{\text{p,leaky}}$ (s·m^{-3})
66.208	−17.252	2.055×10^{-2}	0.0405	1.257×10^{3}
66.803	−12.838	1.001×10^{-2}	0.123	1.880×10^{3}
67.304	−5.284	4.318×10^{-3}	0.381	2.504×10^{3}
67.693	−1.931	1.634×10^{-3}	1.125	2.804×10^{3}
67.954	−0.488	4.170×10^{-4}	3.345	2.129×10^{3}
68.178	−0.001	1.421×10^{-6}	8548.103	1.860×10^{4}

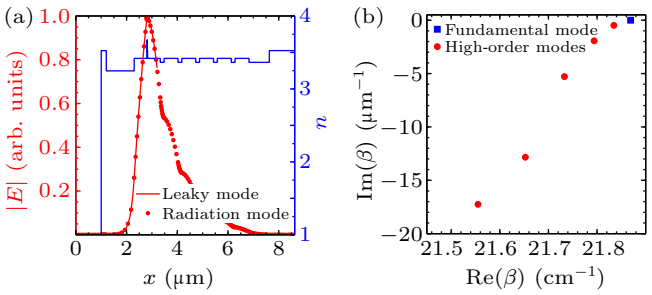


Fig. 3. (a) The red solid line is the normalized distribution of the electric field of the fundamental leaky mode, the red points are the normalized electric field distribution of the radiation mode at the mode angle of the leaky mode, and the blue solid line is the distribution of the refractive index of the 1D waveguide. (b) The distribution of the complex propagation constants of the leaky modes in the complex plane. The blue square point stands for the fundamental leaky mode, and the red circle points stand for the high-order leaky modes. Here, Im represents the imaginary part of a complex number.

Furthermore, the ERM is adopted to justify the above results. The mode angle of the leaky mode in the i-th layer is defined as

$$\theta_{\text{leaky}} = \arcsin\left(\frac{\beta_r}{k_0 n_i}\right). \tag{23}$$

The first column in Table 1 is the mode angle in the QW for different leaky modes, which is calculated by Eq. (23). Then, a plane wave E_0 in the QW is used to stimulate the radiation mode of the PBC waveguide, the incident angle θ of which is equal to the mode angle of the fundamental leaky mode. Based on Eq. (12) and the continuity conditions of the tangential components of the electromagnetic fields, the distribution of the normalized electric field of the radiation mode is calculated and shown by the red circle points in Fig. 3(a). For

easier comparison, each mode in Fig. 3(a) is normalized with respect to the maximum of its electric field. The distribution of the normalized electric field of the radiation mode agrees well that of the fundamental leaky mode, except for the small discrepancy in the outmost layers, which results from the different boundary conditions in outmost layers for the two kinds of modes. Only the outgoing waves exist in the outmost layers for the leaky modes, but both the incoming waves and the outgoing waves exist in the outmost layers for the radiation modes.

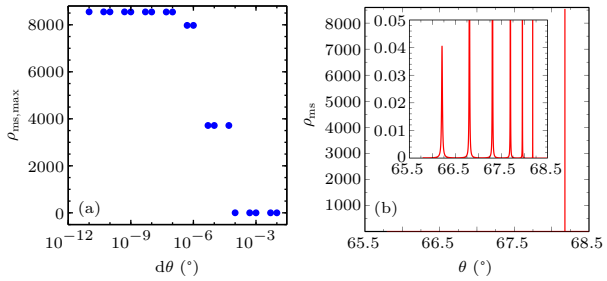


Fig. 4. (a) The maximum of the mode spectrum in the QW, with the incident angle around the mode angle of the fundamental leaky mode, *versus* the accuracy of the angle sweeping. (b) The mode spectrum in the QW *versus* the incident angle of the initial plane wave E_0 when the accuracy of the angle sweeping is $1\times10^{-7\circ}$. The inset is the amplified figure.

The strong confinement of the radiation mode in the inner layers of the waveguide indicates that there is a strong resonance at the mode angle of the leaky mode. This result is proved again by the mode spectrum in the QW around these mode angles. Figure 4(a) shows that the maximum of the mode spectrum in the QW, $\rho_{\mathrm{ms,max}}$, with the incident angle around the mode angle of the fundamental leaky mode, converges when the accuracy of the angle sweeping is higher than $1\times10^{-7\circ}$. Therefore, the accuracy of the angle sweeping is chosen to be $1\times10^{-7\circ}$ to calculate the mode spectrum. The mode spectrum in the QW, calculated by Eq. (8), is shown in Fig. 4(b), which indicates the strong resonances indeed appear around the mode angles in the first column of Table 1. The third column of Table 1 is the full width at half maximum (FWHM) of these resonances. The lower the order of the leaky mode is, the narrower the FWHM of the corresponding resonance is. Hence, the mode spectrum can characterize the radiation loss of the leaky mode. The narrower the FWHM of the resonance emerged in the mode spectrum is, the smaller the leaky loss of the corresponding leaky mode experiences. The resonance, corresponding to the fundamental leaky mode, possesses the narrowest FWHM of $1.421\times10^{-6\circ}$, and the largest maximum of the mode spectrum of 8548.103, as shown in the fourth column of Table 1. Besides, in order to characterize the DOS around the resonance, $\rho_{\mathrm{p,leaky}}$, the range of the integral in Eq. (11) is chosen from ($\theta_{\mathrm{leaky}}-\mathrm{FWMH}$) to ($\theta_{\mathrm{leaky}}+\mathrm{FWMH}$). The calculated results are presented in the fifth column of Table 1, indicating that the fundamental leaky mode has the largest $\rho_{\mathrm{p,leaky}}$ of 1.860×10^{4} s·m^{-3}. These results explain why the PBC laser exclusively operates in the fundamental leaky mode.[36]

3.2. DOS and LDOS

After the radiation modes and the mode spectrum are determined, the DOS and the LDOS in the PBC waveguide can be solved according to Eqs. (11) and (20). Because the refractive index of the QW is higher than that of the substrate layer, and the there are no guided modes existing between the two refractive indices, the range of integral of the incident angle in QW is from 0° to $\arcsin(n_{\mathrm{s}}/n_{\mathrm{qw}})=73.642^{\circ}$ when the total DOS and total LDOS are calculated in the QW. n_{s} is the refractive index of the substrate layer, and n_{qw} is the refractive index of the QW. For the other layers in the PBC waveguide, their refractive indices are all smaller than that of the substrate layer, so the range of the integral of the incident angle is from 0° to 90°. Due to the even symmetry of integrals in Eqs. (11) and (20) with respect to 90°, the calculated results must be multiplied by 2. In view of the memory of the computer, the accuracy of angle sweeping is set to be $1\times10^{-7\circ}$ from ($\theta_{\mathrm{leaky}}-1\times10^{-4\circ}$) to ($\theta_{\mathrm{leaky}}+1\times10^{-4\circ}$), and the accuracy of angle sweeping is set to be $1\times10^{-4\circ}$ for the rest of angles. In this way, the total DOS and the total LDOS can be calculated correctly and quickly. In Fig. 5(a), the red solid line with circle points is the total DOS in the QW as a function of the wavelength, which is enhanced by the effective resonator, relative to that in vacuum, as shown by the blue solid line with diamond points. However, there is no obvious modulations on the DOS in the QW by the PBC waveguide, because the integral in Eq. (11) incorporates all the possible directions of the optical waves. Although the photonic band of the infinite PBC has some forbidden bands in some wavelength intervals for a specified mode angle, these wavelength intervals will vary if the mode angle changes. For the infinite PBC with the same parameters as the finite PBC in Fig. 2, a forbidden band appears in the wavelength interval, ranging from 782 nm to 941 nm, as shown in Fig. 6(a), when the mode angle is fixed at 85° in the layer with the lower refractive index. When the mode angle is changed to 65°, the location of the forbidden band also changes, which ranges from 1051 nm to 1078 nm, as shown in Fig. 6(b). In the two cases, the forbidden bands do not overlap, so there are no perfect forbidden bands, inhibiting the propagation of every direction optical wave, in the wavelength range of interests, which leads to the weak modulations on DOS.[40] In order to further investigate the DOS within different layers, the wavelength is fixed at 980 nm. Figure 5(b) is the distribution of the DOS in different layers of the PBC waveguide. The DOS in different layers is different from each other, and the DOS in the outmost layers is equal to that in the corresponding uniform medium. Therefore, the DOS defined by Eq. (11) indeed reveals the partial spatial dependence of the

LDOS,[27] but the information of the LDOS inside each layer is still missed, and can be characterized by Eq. (20).

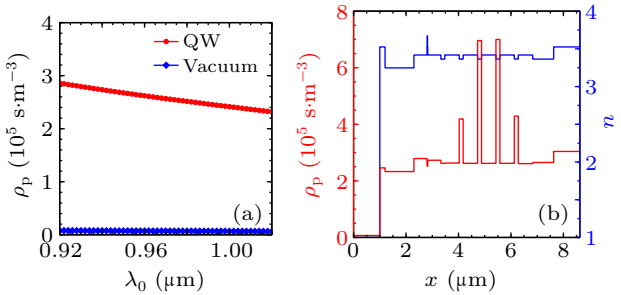


Fig. 5. (a) The DOS *versus* the wavelength. The red solid line with circle points is the DOS in the QW, and the blue solid line with diamond points is the DOS in vacuum. (b) The red solid line is the DOS in the QW *versus* x when the wavelength in vacuum is fixed at 980 nm, and the blue solid line is the distribution of the refractive index.

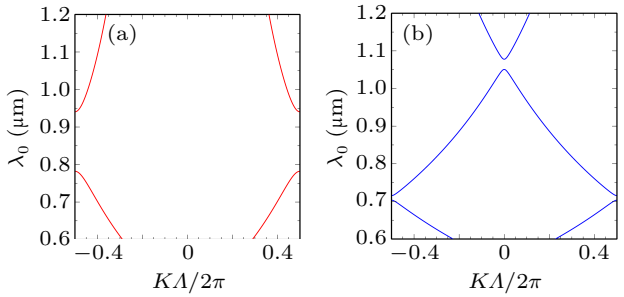


Fig. 6. (a) The red solid line is the photonic band of the infinite PBC with same parameters as the finite PBC in Fig. 2 when the mode angle is fixed at 85° in the layer with the lower refractive index. K is the Bloch wave vector, and Λ is the period of the PBC, equal to 0.7 μm. (b) The blue solid line is the photonic band of the same infinite PBC when the mode angle is fixed at 65° in the layer with the lower refractive index.

As discussed before, the DOS cannot reveal the dependence of the number of modes on space inside each layer. Therefore, in order to remove this deficiency, the electric field of the radiation mode should be set as the weighting function when the number of modes is counted in each layer, the result of which is the LDOS given by Eq. (20). According to the Eqs. (12) and (20), the LDOS of each layer at the wavelength of 980 nm is calculated and illustrated in Fig. 7(a). From Fig. 7(a), it can be known that the LDOS slowly varies with the position in the wider layers, but sharply varies with the position in the narrower layer, especially in the PBC layer with the lower refractive index. The LDOS asymptotically approaches the DOS in the uniform media as the position gets away from the PBC waveguide.

Then, the influence of the location of the active layer on the DOS and the LDOS is investigated. Here, the total LDOS means the integral include all possible incident angles, while the partial LDOS means the integral only includes the incident angles around the mode angle of the fundamental leaky mode. The red dashed line in Fig. 7(b) is the total DOS in the QW as a function of the location of the interface between the left defect layer and the left quantum barrier, which is an average of the total LDOS in the QW, shown by the grey points in Fig. 7(b). As the location of the active layer changes, the total DOS changes little, which means the total spontaneous emission rate changes little. However, the distribution of the LDOS in the QW sharply varies as the location of the active layer changes. Especially, when the QW is located at the center of the defect layer, the LDOS distributes extremely inhomogeneous in the QW, which results in the nonuniform spontaneous emission rate in the QW, and aggravates the performances of active devices, such as the saturate power of lasers.[36] Therefore, the QW should be placed off the center of the defect layer. Finally, the partial DOS and the partial LDOS around the mode angle of the fundamental leaky mode are also calculated, the integral range of the incident angle of which is reset to be from $(\theta_{\text{leaky}} - 1 \times 10^{-4\circ})$ to $(\theta_{\text{leaky}} + 1 \times 10^{-4\circ})$ for simplicity. The more accurate of the integral range should be obtained by further calculations or experiments. The black solid line in Fig. 7(b) is the partial DOS, and the green points are the partial LDOS, both of which exhibit the same behavior with respect to the location of the QW. When the position of the interface between the left defect layer and the left quantum barrier is chosen to be near 2.91 μm, both the partial DOS and the partial LDOS obtain the maximal value, which means more spontaneous photons around the mode angle of the fundamental leaky mode can be coupled into the fundamental lasing mode of lasers, enhancing the output power of the lasing mode. Even though the calculations here are passive, these results can be applied to the actual active devices when the electrical and thermal factors are incorporated in the future.

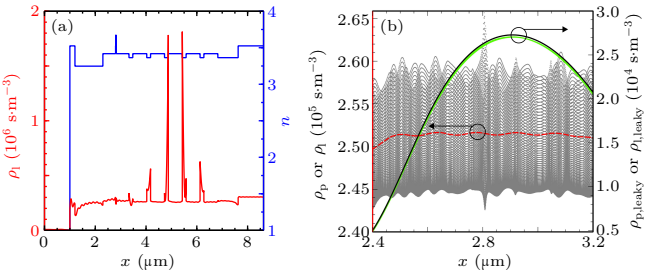


Fig. 7. (a) The red solid line is the LDOS *versus* x when the wavelength in vacuum is fixed at 980 nm, and the blue solid line is the distribution of the refractive index. (b) The DOS and the LDOS in the QW *versus* the location of the interface between the left defect layer and the left quantum barrier when the wavelength in vacuum is fixed at 980 nm. The grey points are the total LDOS. The red dashed line is the total DOS, which is a good average of the total LDOS. The green points are the partial LDOS, and the black solid line is the partial DOS, both of which are calculated by integrating the incident angle around the mode angle of the fundamental leaky mode in the QW.

4. Conclusion

In summary, the method of calculating the LDOS in 1D stratified media is proposed in this work. The relationship between the mode spectrum and the LDOS is established mathematically, which shows that the LDOS is the integral of the mode spectrum, weighted by the electric field of the radiation mode, in the angular space. Because the electric field pos-

sesses the information of spatial positions, the LDOS can reveal the dependence of the number of modes on the space. By adopting the effective resonator model and the transfer matrix method, the analytical expressions of the mode spectrum, the electric field, the DOS and the LDOS are established. The mode spectrum can characterize the leaky loss of the leaky mode, and the narrower the FWHM of the resonance in the mode spectrum is, the smaller the leaky loss of the corresponding leaky mode experiences. The PBC studied here has no obvious modulations on the DOS in QW in the wavelength space, because the DOS has incorporated the contributions of all the possible directions of optical waves at each wavelength, and there are no perfect forbidden bands in the wavelength range of interests. The DOS defined here is different for different layers, but still misses the spatial information inside each layer. The calculated LDOS can reveal the spatial information inside each layer, which shows that the QW should be placed off the center of the defect layer for active devices, due to the extremely inhomogeneous distribution of the LDOS in the QW at this position. Finally, the partial DOS and the partial LDOS, related to the fundamental leaky mode, indicate that there is an optimal position of the QW in the defect layer, which should be further studied by considering the electrical and thermal factors in the future. In our future works, some improvements will also be considered in calculating the LDOS in 1D stratified media. Firstly, although there are no guided modes in the PBC waveguide in our case because of the high refractive index of the substrate, the integral in Eq. (20) should be discretized if the guided modes appear. Secondly, the evanescent waves can penetrate the layer with the lower refractive index when the total reflection happens between adjacent layers, which means that the mode angle in the layer with the lower refractive index becomes complex. Therefore, the formula to calculate the LDOS in the layer with the lower refractive index should be reconstructed due to the existence of the complex mode angle. Nevertheless, our work may offer new insights for the designs of active devices based on the LDOS.

Acknowledgments

Ting Fu thanks Dr Jeremy Sanders for his free software, Veusz, for graphing. Ting Fu also thanks Dr Zhigang Song from the Institute of Semiconductors for the useful discussion about the calculations of the LDOS.

Project supported by the National Key Research and Development Program of China (Grant Nos. 2021YFA1400604 and 2021YFB2801400) and the National Natural Science Foundation of China (Grant Nos. 91850206, 62075213, 62135001, and 62205328).

References

[1] Yablonovitch E 1987 *Phys. Rev. Lett.* **58** 2059
[2] Fan S, Villeneuve P R, Joannopoulos J D and Schubert E F 1997 *Phys. Rev. Lett.* **78** 3294
[3] Purcell E M 1946 *Phys. Rev.* **69** 674
[4] Sprik R, van Tiggelen B A and Lagendijk A 1996 *Europhys. Lett.* **35** 265
[5] de Dood M J A, Slooff L H, Polman A, Moroz A and van Blaaderen A 2001 *Phys. Rev. A* **64** 033807
[6] Wang Q, Stobbe S and Lodahl P 2011 *Phys. Rev. Lett.* **107** 167404
[7] Jiang B, Zhang Y J, Zhou W J, Chen W, Liu A J and Zheng W H 2011 *Chin. Phys. B* **20** 24208
[8] McPhedran R C, Botten L C, McOrist J, Asatryan A A, de Sterke C M and Nicorovici N A 2004 *Phys. Rev. E* **69** 016609
[9] Pickering T, Hamm J M, Page A F, Wuestner S and Hess O 2014 *Nat. Commun.* **5** 4972
[10] Vahala K J 2003 *Nature* **424** 839
[11] Mignuzzi S, Vezzoli S, Horsley S A R, Barnes W L, Maier S A and Sapienza R 2019 *Nano Lett.* **19** 1613
[12] Martín-Jiménez A, Fernández-Domínguez A I, Lauwaet K, Granados D, Miranda R, García-Vidal F J and Otero R 2020 *Nat. Commun.* **11** 1021
[13] Moroz A 1999 *Europhys. Lett.* **46** 419
[14] Wubs M and Lagendijk A 2002 *Phys. Rev. E* **65** 046612
[15] Yeganegi E, Lagendijk A, Mosk A P and Vos W L 2014 *Phys. Rev. B* **89** 045123
[16] Mavidis C P, Tasolamprou A C, Hasan S B, Koschny T, Economou E N, Kafesaki M, Soukoulis C M and Vos W L 2020 *Phys. Rev. B* **101** 235309
[17] Losquin A and Kociak M 2015 *ACS Photon.* **2** 1619
[18] Zu S, Han T, Jiang M, Lin F, Zhu X and Fang Z 2018 *ACS Nano* **12** 3908
[19] Zu S, Han T, Jiang M, Liu Z, Jiang Q, Lin F, Zhu X and Fang Z 2019 *Nano Lett.* **19** 775
[20] Asatryan A A, Busch K, McPhedran R C, Botten L C, Martijn de Sterke C and Nicorovici N A 2001 *Phys. Rev. E* **63** 046612
[21] Huang Y G, Fan H and Wang X H 2010 *Chin. Phys. Lett.* **27** 104213
[22] Forati E 2022 *IEEE J. Multiscale Multiphys. Comput. Tech.* **7** 46
[23] Rudziński A, Tyszka-Zawadzka A and Szczepański P 2005 *Proc. SPIE, October 12, 2005, Warsaw, Poland*, p. 59501A
[24] Rudziński A 2007 *Acta Phys. Pol. A* **111** 323
[25] Rudziński A, Tyszka-Zawadzka A and Szczepański P 2007 *Opt. Quantum Electron.* **39** 501
[26] Rudziński A and Szczepański P 2010 *Photon. Lett. Pol.* **2** 79
[27] Baradaran Ghasemi A H, Khorasani S, Latifi H and Atabaki A H 2010 *Wave. Random Complex* **20** 419
[28] Yeh P 1988 *Optical Waves in Layered Media* (New York: John Wiley & Sons) pp. 102–117
[29] Carminati R, Cazé A, Cao D, Peragut F, Krachmalnicoff V, Pierrat R and De Wilde Y 2015 *Surf. Sci. Rep.* **70** 1
[30] Bendickson J M, Dowling J P and Scalora M 1996 *Phys. Rev. E* **53** 4107
[31] Benech P, Khalil D A M and André F S 1992 *Opt. Commun.* **88** 96
[32] Gerard P, Benech P, Ding H and Rimet R 1994 *Opt. Commun.* **108** 235
[33] Ledentsov N N and Shchukin V A 2002 *Opt. Eng.* **41** 3193
[34] Maximov M V, Shernyakov Y M, Novikov I I, Karachinsky L Y, Gordeev N Y, Ben-Ami U, Bortman-Arbiv D, Sharon A, Shchukin V A, Ledentsov N N, Kettler T, Posilovic K and Bimberg D 2008 *IEEE J. Sel. Top. Quantum Electron.* **14** 1113
[35] Liu L, Qu H, Liu Y, Zhang Y, Wang Y, Qi A and Zheng W 2014 *Appl. Phys. Lett.* **105** 231110
[36] Chen Z, Qi A, Zhou X, Qu H, Chen J, Jia Y and Zheng W 2021 *IEEE Photon. Technol. Lett.* **33** 399
[37] Benech P and Khalil D 1995 *Opt. Commun.* **118** 220
[38] Hu J and Menyuk C R 2009 *Adv. Opt. Photon.* **1** 58
[39] Zhu L, Scherer A and Yariv A 2007 *IEEE J. Quantum Electron.* **43** 934
[40] Alvarado-Rodríguez I, Halevi P and Sánchez-Mondragón J J 1999 *Phys. Rev. E* **59** 3624